Engineering Structures 219 (2020) 110745

Contents lists available at ScienceDirect

Engineering Structures

journal homepage: www.elsevier.com/locate/engstruct

A study of the effects of foundation uplift on the seismic loading of wind turbine tower and shallow foundation using a new dynamic Winkler model

Lilin Wang, Takeshi Ishihara*

Department of Civil Engineering, School of Engineering, The University of Tokyo, 7-3-1, Hongo, Bunkyo-ku, Tokyo, Japan

ARTICLE INFO

Keywords:
Foundation uplift
Seismic loading
Wind turbine tower
Shallow foundation
Dynamic Winkler model

ABSTRACT

In this study, the effects of foundation uplift on the seismic loading of wind turbine tower and shallow foundation are investigated. A dynamic Winkler model is proposed for the dynamic response analysis of shallow foundation supported structures and is named as QzSimple4, in which PySimple3 is applied to replace the elastoplastic component in QzSimple2 for the compression under the foundation and the gap model in QzSimple1 is assembled to capture the foundation uplift. The proposed model agrees well with the q-z experimental backbone curves and reasonably captures the acceleration responses of the bridge deck and the settlement-rotation responses of the shallow foundation under various excitation levels. However, QzSimple2 model strongly overestimates the q-z backbone curves in terms of linear range and ultimate bearing capacity, which leads to obviously overestimate some acceleration responses of the bridge deck and significantly underestimate the settlement responses of the shallow foundation. Finally, a systematical study is performed to investigate the effects of foundation uplift on the seismic loading by using the proposed Winkler model and the equivalent linear sway-rocking model. The foundation uplift occurs under severe earthquakes. Without considering the foundation uplift, the moment on the wind turbine tower is slightly overestimated, while that on the shallow foundation is significantly underestimated for the large soil stiffness. This is one reason why the shallow foundations at Aso-Nishihara wind farm were damaged during the Kumamoto earthquake.

1. Introduction

As stated in DNVGL [1], it is necessary to consider the fatigue limit state (FLS), the ultimate limit state (ULS) as well as the accidental limit state (ALS) in the design of wind turbine supporting structures. FLS and ULS rely more on the initial stiffness and damping of soil and relate to the cyclic nature of soil (e.g. the degradation of strength and stiffness shown in Allotey and El Naggar [2]) while the ALS focuses on the damage caused by accidental hazards such as typhoon and earthquakes. This study focuses on the damage of wind turbine supporting structures caused by the Kumamoto earthquake. About 90% shallow foundations of wind turbines at the Aso-nishihara wind farm in Kumamoto, Japan were damaged due to the Kumamoto earthquake, while all wind turbine towers are safe [3]. The damage analyses of shallow foundations at the Aso-nishihara wind farm indicated that the response under the shallow foundation during the strong earthquake was nonlinear and the strong foundation uplift was involved. In the current JSCE guideline [4], the equivalent linear sway-rocking model (SR model) is adopted, which approximately considers the nonlinear soil-structure interaction using the equivalent soil stiffness and damping, but does not consider the effects of foundation uplift. The questions arise that what the effects of foundation uplift are on the safety of wind turbine supporting structures and what will happen during the strong earthquake if the foundation uplift is not considered in the design.

In terms of modelling the soil-structure interaction of shallow foundation, a great many researches have been performed in the past decades, which can be categorized as sway-rocking model (also known as macroelement model, e.g. Chatzigogos et al. [5], Figini et al. [6]) and Winkler model (e.g. Allotey and El Naggar [7-9], Raychowdhury and Hutchinson [10]). The Winkler model in Raychowdhury and Hutchinson [10] is focused in this study since it is popular and available in the open-source software OpenSees [11]. A set of well-formed models, such as PySimple1 [12], QzSimple1 [13] and TzSimple1 [14], were proposed for a beam on nonlinear Winkler foundation (BNWF) analysis of pile foundation by fitting to the static and slow cyclic tests (e.g. the API sand p-y model) by Boulanger et al. [15]. These models were recalibrated for the BNWF analysis of shallow foundation by the static and slow cyclic tests by Raychowdhury and Hutchinson [10], which are known as PySimple2, QzSimple2 and TzSimple2. The geometrical nonlinearities of soil-structure interaction are also included in these models, such as the

* Corresponding author.
E-mail address: ishihara@bridge.t.u-tokyo.ac.jp (T. Ishihara).

https://doi.org/10.1016/j.engstruct.2020.110745
Received 5 February 2020; Received in revised form 26 April 2020; Accepted 3 May 2020

gap model in PySimple1 for the separation behavior of pile foundation and the gap model in QzSimple2 for the uplifting behavior of shallow foundation. However, Choi et al. [16] pointed out that the API sand p-y model (also for PySimple1) is not suitable for the dynamic analysis of pile foundation in terms of ultimate bearing capacity, initial stiffness as well as the shape of p-y backbone curve and proposed the PySimple3 model to better capture the nonlinear p-y behavior of pile foundation in sand during earthquake loading. It is doubted whether the QzSimple2 model can capture the nonlinear behavior under shallow foundation and the BNWF analysis with QzSimple2 can predict the dynamic responses of the whole system during earthquake loading.

Many researches (see Katsanos, et al.[17]) focused on the seismic implications on the wind turbine since numerous wind turbines are installed in the earthquake active areas. Bazeos et al.[18] studied the seismic behavior of a steel tower for a 450 kW 38 m high wind turbine with a set of linear springs and dashpots at the soil-foundation interface of the finite element model, and pointed out the effects of soil-structure interaction (SSI) on the fundamental frequency of wind turbine tower, on the higher vibrational modes in terms of their shapes and the corresponding natural frequencies. The importance of SSI effect on the seismic responses of wind turbine towers and foundations were also mentioned by several other researches (e.g. Zhao and Maißer [19], Butt and Ishihara [20]). However, these researches did not investigate the effects of foundation uplift on the seismic loading of wind turbine supporting structures. Recently, the damages of shallow foundations at the Aso-nishihara wind farm due to the Kumamoto earthquake were analyzed by a Winkler model with the spring model assembled by trilinear model and gap model, but the effect of foundation uplift on the seismic loading of wind turbine towers was not investigated. In addition, some researches (see Richard [21], Czerewko et al. [22], Cabalar et al.[23] and Schneider and Senders[24]) investigated how the geological formation affects the design of wind turbine supporting structures. The geological formation of the Aso-nishihara wind farm can be found in Reference [3].

In this study, the effects of foundation uplift on the seismic loading of wind turbine tower and shallow foundation are investigated using a new dynamic Winkler model, which is proposed in Section 2. The proposed Winkler model is then validated by a series of shaking table tests in Section 3. The effects of foundation uplift on the seismic loading of wind turbine supporting structures are investigated in Section 4. Conclusions are given in Section 5.

2. A new dynamic Winkler model for shallow foundations

The response of a shallow foundation is usually analyzed using the beam on the nonlinear Winkler foundation (BNWF) approach. A new dynamic Winkler model for the shallow foundation supported structure is illustrated in Fig. 1. In the Winkler model, the soil-shallow foundation interaction is modeled with multiple distributed q-z springs and two horizontal springs (known as p-x spring and t-x spring) (see Fig. 1b). Note that the terminologies “q-z spring, p-x spring and t-x spring” are named according to the coordinate in Fig. 1b, which are the sames as those in Raychowdhury and Hutchinson [10]. The q-z springs in the vertical direction captures the vertical and rocking behaviors under the vertical resistance of a shallow foundation, the p-x spring is used for the sliding behaviour under the passive side resistance of an embedded shallow foundation, while the t-x spring is for the sliding behaviour under the frictional resistance along the base of a shallow foundation. As shown in Fig. 1c, the proposed q-z spring (referred as QzSimple4) is obtained by combining a gap component in QzSimple1 and an elastoplastic component in PySimple3, which yields a fully compressed behavior in the negative side, but a reduced uplift behavior in the positive side.

Note that the soil damping includes hysteretic damping, radiation damping as well as small-strain damping. The small-strain damping is needed since soil is known to exhibit damping even at the smallest levels of measurable strain (e.g., Vucetic and Dobry [25]), which is 2% in JSCE guideline [4]. One way to consider the three types of soil damping is depicted in Turner [26], the hysteretic damping is captured by the hysteretic loops of the PySimple3 model, the radiation damping is accounted for by adding a viscous dashpot in parallel with an elastic spring in the PySimple3 model and the small-strain damping is incorporated with structural damping by Rayleigh damping. In this study, the hysteretic damping, the small-strain damping and the structural damping are considerred as same as those in Turner [26], but the radiation damping is not considered to keep consistent with Choi et al. [16]. Another reason why the radiation damping is not added is that the radiation damping is usually not accounted in the equivalent linear SR model (see JSCE guideline [4]).

2.1. Constitutive relationships of q-z, t-x and p-x springs

As illustrated in Fig. 1c, the proposed q-z spring is assembled by an elastoplastic component and a gap component. The governing equations of PySimple3 are adopted for the elastoplastic component as described in Eqs. (1)–(5) and those of the gap model in QzSimple1 are used for the gap component as shown in Eqs. (6) and (7).

The PySimple3 model proposed by Choi et al. [16] is adopted for the elastoplastic component of the proposed q-z spring to capture the compression and rotation behavior of soil-structure interaction. The elastic constitutive law (Eq. (1)), the yield function (Eq. (2)), the plastic modulus definition (Eq. (3)), the kinematic hardening law (Eq. (4)), the elastoplastic modulus K (Eq. (5)) of the PySimple3 model are presented herein briefly.

$$\dot{q} = K_e \dot{z}_e = K_e(\dot{z} - \dot{z}_p) \tag{1}$$

$$f = |q - q_\alpha| - q_y \tag{2}$$

$$K_p = C \cdot K_e \frac{|[q_u \cdot sign(\dot{z})] - q|}{|q - q_{in}|} \tag{3}$$

$$\dot{q}_\alpha = K_p \dot{z}_p \tag{4}$$

$$K = \frac{\dot{q}}{\dot{z}} = \frac{K_e K_p}{K_e + K_p} \tag{5}$$

where K_e is the elastic modulus, K_p is the plastic modulus; f is the yield function; q_α is the value of q at the center of the elastic region (analogous to the backstress in the classical plasticity theory), q_y is the yielding force, q_{in} is the value of q at the start of current plastic loading cycle and q_u is the ultimate bearing capacity; C is the hardening material constant; $\dot{z}_e$ is the elastic displacement rate, $\dot{z}_p$ is the plastic displacement rate, $\dot{z}$ is the displacement rate.

The gap model in QzSimple1 (see Boulanger [13]) is adopted for the gap component of the proposed q-z spring to capture the behavior of foundation uplift, which consists of a closure element and a drag element in parallel. The closure element is a bilinear elastic spring, which is relatively stiff in compression and very flexible in tension (see Eq. (6)) and the drag component is modeled with a hyperbolic spring (see Eq.(7)).

$$q_c = \begin{cases} 0.001 \frac{q_u}{z_{50}} z_g & (z_g > 0) \\ 1000 \frac{q_u}{z_{50}} z_g & (z_g \leqslant 0) \end{cases} \tag{6}$$

$$q_d = C_d q_u - (C_d q_u - q_{in}^d)\left(\frac{z_{50}}{z_{50} + 2\,|z_g - z_{in}^g|}\right) \tag{7}$$

where q_c and q_d are the forces in the closure element and the drag element respectively, q_{in}^d is the value of q_d at the start of current plastic loading cycle, z_{in}^g is the value of z_g at the start of current plastic loading cycle and is the suction ratio, which means the ratio of the maximum suction force to the ultimate bearing capacity of the q-z nonlinear

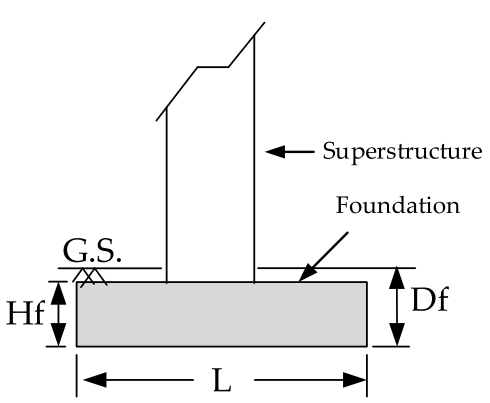

(a) Shallow foundation supported structure

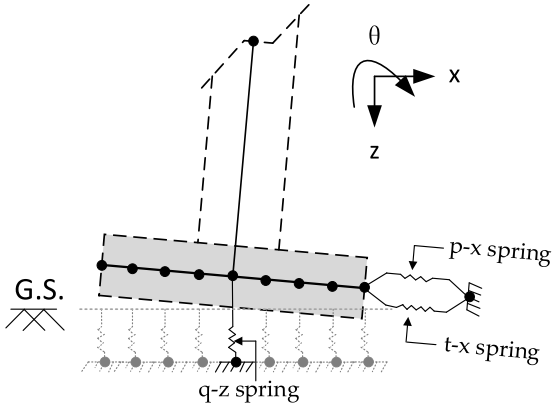

(b) Winkler model for the shallow foundation supported structure

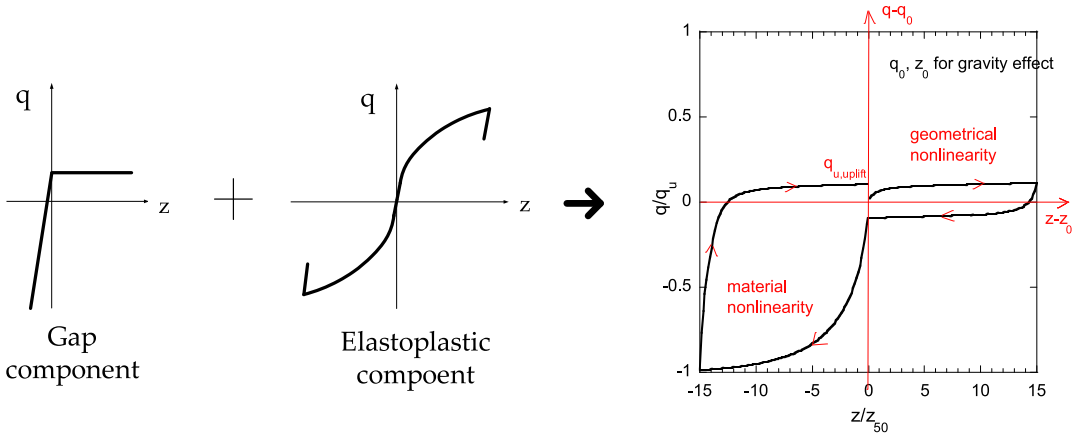

(c) Illustration of the q-z spring

Fig. 1. Shallow foundation supported structure and its models.

spring; z_{50} is the value of z where q equals to $0.5q_u$.

The governing equations of the p-x and t-x springs are similar to those of the q-z spring. More specifically, the same elastoplastic component is used in both p-x and t-x springs. In terms of the gap component of the p-x spring, the drag element is the same as that in the q-z spring (see Eq.(7)), but the closure element is governed by Eq. (8) (see Boulanger [12]). Note that no gap component exists in the t-x spring.

$$p_c = 1.8p_u\left(\frac{y_{50}}{y_{50} + 50(y_0^+ - y_g)} - \frac{y_{50}}{y_{50} - 50(y_0^- - y_g)}\right) \tag{8}$$

where y_0^+ is the memory term for the positive side of the gap, y_0^- is the memory term for the negative side of the gap. The initial values of y_0^+ and y_0^- are $y_{50}/100$ and $-y_{50}/100$, respectively. y_{50} is the value of y where p equals to $0.5p_u$.

2.2. Description of input parameters

The input parameters for the q-z spring and the references to determine these parameters are summarized in Table 1. The ultimate bearing capacity q_u of the whole rectangular foundation is calculated by Eq. (9), which follows Meyerhof [27].

$$q_u = (cN_cF_{cs}F_{cd}F_{ci} + \gamma D_f N_q F_{qs}F_{qd}F_{qi} + 0.5\gamma BN_\gamma F_{\gamma s}F_{\gamma d}F_{ri})LB \tag{9}$$

where c is cohesion, γ is the unit weight of soil, D_f is the depth of embedment, L is the length of foundation, B is the width of foundation; N_c, N_q and N_γ are the bearing capacity factors, F_{cs}, F_{qs} and $F_{\gamma s}$ are the shape factors, F_{cd}, F_{qd} and $F_{\gamma d}$ are the depth factors, F_{ci}, F_{qi} and F_{ri} are the inclination factors. These factors are the functions of soil friction angle

Table 1
The input parameters for the proposed q-z spring.

Parameters in q-z spring and their locations		References to determine parameters
q_u	Elastoplastic component	Meyerhof [27]
K_{eq}		Gazetas [28]
q_y		Kagawa and Kraft [29] and Darendeli [30]
C		Choi et al. [16]
z_{50}	Gap component	Raychowdhury [31]
C_d		Raychowdhury[31]

ϕ and can be found in Meyerhof [27]. In this study, the dynamic values of friction angle and cohesion (known as ϕ_{dynamic} and c_{dynamic}) rather than the static values (known as $\phi_{\text{static}}$and c_{static}) are adopted to calculate the ultimate bearing capacity q_u, which is a major difference from the previous models and the reason why the dynamic Winkler model is used. The rate effect on the ultimate bearing capacity of shallow foundation was proved by Vesic et al. [32] for the dense sand and by Carroll [33] for the buckshot clay by experiments. Moreover, Vesic [47] suggested that the minimum value of q_u in granular soil can be obtained by using ϕ_{dynamic} equaling to $\phi_{\text{static}} - 2^\circ$. It is suggested that the values of ϕ_{dynamic} and c_{dynamic} can be determined by Eqs. (10) and (11).

$$\phi_{\text{static}} - 2^\circ \leqslant \phi_{\text{dynamic}} < \phi_{\text{static}} \tag{10}$$

$$c_{\text{dynamic}} \approx 1.5c_{\text{static}} \tag{11}$$

where $\phi_{\text{dynamic}}$and c_{dynamic} are the values under the dynamic condition while ϕ_{static} and c_{static} are the values under the static condition.

The elastic spring stiffness K_{eq} can be determined according to Gazetas [28] for the rectangular foundation or the Cone model (see JSCE guideline [4]) for the circular foundation. K_{eq} in Gazetas [28] is shown in Eq.(12).

$$K_{eq} = \frac{GL}{1-\upsilon}\left[0.73 + 1.54\left(\frac{B}{L}\right)^{0.75}\right] \tag{12}$$

where G is the initial shear modulus of soil, υ is the Poisson ratio of soil.

The yielding force q_y is expressed by Eq. (13).

$$q_y = K_{eq} z_{\text{yield}} \tag{13}$$

where $z_{\text{yield}} = 2.5B\gamma_{\text{yield}}/(1+\upsilon)$ (Kagawa and Kraft [29]), $\gamma_{\text{yield}} = 0.001\%$ (Darendeli [30]); z_{yield}, γ_{yield} are the displacement and the soil strain where the yielding force occurs.

The hardening material constant C has been proposed for pile foundation by Choi et al. [16] and the same equation is adopted for shallow foundation as shown in Eq. (14). This is because the Winkler modelling of shallow foundation can be analogy with that of pile foundation.

$$C = \frac{(q_u - q_y)[\ln(q_u - q_y) - \ln(q_u)] + q_u[\ln(2) - 0.5] + q_y[1 - \ln(2)]}{K_{eq} z_{50} - 0.5 q_u} \tag{14}$$

z_{50} is the value of z where q equals to $0.5q_u$ and is usually obtained from experiments. When the experimental data are not available, z_{50} can be determined by Eq. (15) (see Raychowdhury [31]).

$$z_{50} = k_f \frac{q_u}{K_{eq}} \tag{15}$$

where k_f is a non-dimensional coefficient, which is calibrated via a series of static shallow foundation tests in Raychowdhury [31]. It is assumed that the same values can be used for the dynamic analysis.

The suction coefficient C_d is usually chosen from the range of $0 \sim 0.1$. The input parameters for the p-x and t-x springs can be determined similarly to those for the q-z spring, which are omitted here.

3. Validation of the proposed dynamic Winkler model

The information of shaking table tests is presented in Section 3.1. The q-z spring backbone curve is validated in Section 3.2, and the proposed dynamic Winkler model is investigated in Section 3.3.

3.1. Information of shaking table tests

A series of 1 g experiments (see Drosos et al. [34] and Anastasopoulos et al. [35]) were conducted at the Laboratory of Soil Mechanics of the National Technical University of Athens to investigate three foundation design alternatives representing three levels of design conservatism for a bridge pier-shallow foundation system under the seismic shaking. The shaking table, 1.3 m × 1.3 m in dimensions, is capable of shaking specimens of 2 Mg at accelerations up to 1.6 g. Synthetic accelerograms, as well as real earthquake records can be simulated. The actuator is equipped with a servo-valve, controlled by an analog inner-loop control system and a digital outer-loop controller; it is capable of producing a stroke of ± 75 mm(see Anastasopoulos et al. [36]). Fig. 2 presents the prototype of bridge pier-foundation system, the simplified rigid-structure model showing the notation for loads and displacements, the geometry of the foundation-structure model, the time histories and elastic response spectra of representative sinusoidal excitations. It is noted that considerable difference exists between the targeted input motion and the generated motion especially in the relatively high frequency range due to the limitations in the motion reproduction efficiency of the shaking table (see Anastasopoulos et al. [35]). It is hoped that the differences between the targeted and generated waves are small since the sinusoidal waves are simple with only one dominant frequency.

In this study, two of the three foundation design alternatives, known as large foundation and medium foundation, are employed to validate the proposed Winkler model, the information of which are summarized in Table 2 (see Drosos et al. [34]). The properties of dense dry sand are summarized in Table 3.

3.2. Validation of q-z spring backbone curve

Considering many springs exist in the proposed Winkler model, the accuracy of spring model is a prerequisite of the accuracy of the Winkler model. Fig. 3 portrays the comparisons among the experimental backbone curve, the proposed q-z spring model and the previous QzSimple2 model. The experimental q-z backbone curves are derived from the moment-rotation and settlement-rotation responses corresponding to the Aegion seismic wave, which can be found in Appendix A. The reason why the Aegion seismic wave is selected is due to its characteristically short duration and the presence of a single strong motion pulse. It is found that the proposed q-z spring model shows favorable agreement with experiments for both large and medium foundations. By contrast, the previous spring model QzSimple2 shows a quite large linear range and significantly overestimates the ultimate capacity for both foundations.

3.3. Validation of the proposed dynamic Winkler model

To validate the accuracy of the proposed dynamic Winkler model, numerical analyses are performed for the large foundation in OpenSees [11] by means of the BNWF approach, in which the proposed q-z spring model and the QzSimple2 model are utilized and compared with experimental data. The bridge deck is modelled as a lumped mass and connected to the center of shallow foundation by an elastic beam-column element. The shallow foundation is modeled with 20 elastic beam-column elements evenly distributed along the length of the shallow foundation. Correspondingly, 21 q-z springs are distributed along the shallow foundation at 0.55-m intervals. A t-x spring is connected to the center of shallow foundation in the horizontal direction to mimic the friction at foundation base. Since the shallow foundation rests on the surface of sand layer, no p-x spring is needed. The configuration of the Winkler model formed by QzSimple2 follows the recommendations in Raychowdhury [31]. Input excitations are imposed by using the Multi-Support pattern command, which can yield the absolute values of dynamic responses. The dynamic analyses are performed by using a time step of 10^{-4}, the transformation method for the constraints handler, the reverse Cuthill-McKee scheme for the numberer, the Hilber-Hughes-Taylor method for the integrator, and the energy increment test with a tolerance of 10^{-6} and a max iteration number of 2000. The Rayleigh damping model is adopted to capture the structural damping. Unlike 2% damping is used in Choi et al. [16], a common value of 0.2% for the material damping of steel is adopted since the experimental models are made of steel.

The acceleration responses of bridge deck and the settlement-rotation responses of shallow foundation predicted by the numerical models are compared with experiments in Fig. 4, for which the base excitation is a 12-cycle 2-Hz sine pulse with a 0.15 g acceleration amplitude. For this excitation level, the soil yields but no foundation uplift occurs, which can be seen from the descending slope of the settlement-rotation response. Therefore, it is adopted to validate the capability of the proposed q-z spring to capture the behavior of soil compression. It is noticed that regarding to the acceleration response of bridge deck, the proposed model shows reasonable agreement with the experiment while the previous QzSimple2 model significantly overestimates the maximum value with a relative error of 35%. In terms of the settlement-rotation response of the shallow foundation, the proposed model presents reasonable agreement with the experiment for the settlement response but slightly overestimates the rotation response. This slight

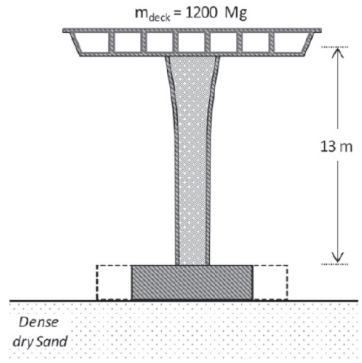

(a) Bridge pier on shallow foundation of varying dimensions (in prototype)

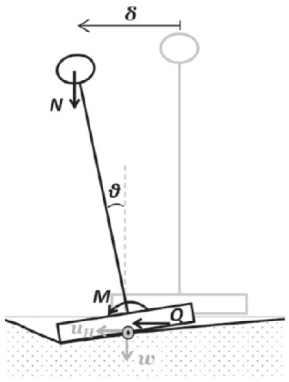

(b) Simplified rigid-structure model with notations for loads and displacements

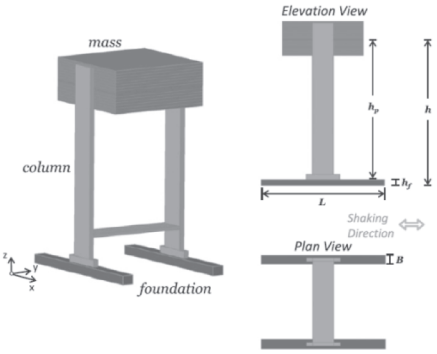

(c) Geometry of the foundation-structure model

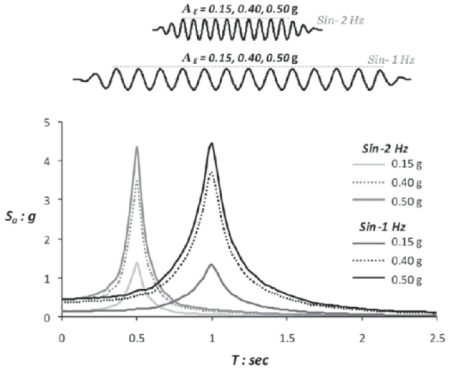

(d) Representative acceleration time histories and their elastic response spectra

Fig. 2. Bridge pier-foundation system and excitation inputs.

Table 2
Properties of large and medium foundations (in prototype).

Property	Large Foundation	Medium Foundation
Bridge deck mass [M (Mg)]	1200	1200
Pier height [H (m)]	13.6	13.6
Column height [hp (m)]	13.0	13.0
Column section area [A (m2)]	1.06	1.06
Column section moment of inertia [Ix (m4)]	0.32	0.32
Foundation length [L (m)]	11.0	7.0
Foundation width [B (m)]	1.7	1.4
Foundation height [H_f (m)]	0.6	0.6
Total vertical load (N (kN))	14,362	13,593
Static safety factor (FSv)	7.49	3.41
Fixed base period [T_0 (s)]	0.16	0.16

Table 3
Summary of soil properties in shaking table tests.

Name	Longstone sand
Relative density Dr (%)	85
Specific weight Gs	2.64
Friction angle (deg)	44
Poisson ratio	0.25
Coefficient of friction	0.7

overestimation may be caused by the soil plastic deformation at the edges of shallow foundation. By contrast, the previous QzSimple2 model does not capture the evolution of the settlement-rotation response at all. This is because that the QzSimple2 model is much stiffer than the proposed model as shown in Fig. 3.

The validation metric (see Schatzmann et al.[37] and Oettl [38]) is introduced to quantify the agreement between experiments and the proposed model, which is presented by a hit rate q and defined by Eq. (16).

$$q = \frac{1}{N}\sum_{i=1}^{N} n_i, \quad \text{with } n_i = \begin{cases} 1, & \left|\frac{y_i - x_i}{x_i}\right| \leqslant D_q \text{ or } |y_i - x_i| \leqslant W_q \\ 0, & \text{else} \end{cases} \tag{16}$$

where x_i and y_i are the values of responses of bridge deck and shallow foundation from experiments and predictions, respectively. For the response of bridge deck, they are the accelerations corresponding to time points between 2 s and 8 s at 0.1-s intervals and for the response of foundation, they are the settlements corresponding to the rotations of 0 rad, −0.5E-3 rad and 0.5E + 3 rad for the 0.15 g acceleration amplitude or those of 0 rad, −1.5E-3 rad and 1.5E + 3 rad for the 0.50 g acceleration amplitude. N is the total number of cases, D_q and W_q are the threshold. Values of the metric corresponding to the complete agreement and disagreement are $q = 1$ and $q = 0$ respectively. As suggested by Schatzmann et al. [37] and Oettl [38] , the thresholds $D_q = 0.25$ and $W_q = 0.1$ |max| are used in this study, in which |max| is a maximum value supposed in the observation. Fig. 5 shows the scatter plots for comparison between the numerical models and the experimental results for the acceleration response of bridge deck and the settlement-rotation response of shallow foundation for the 0.15 g acceleration amplitude, together with the corresponding validation metric boundary. It is observed that the proposed model shows much better performance for the 0.15 g acceleration amplitude than the

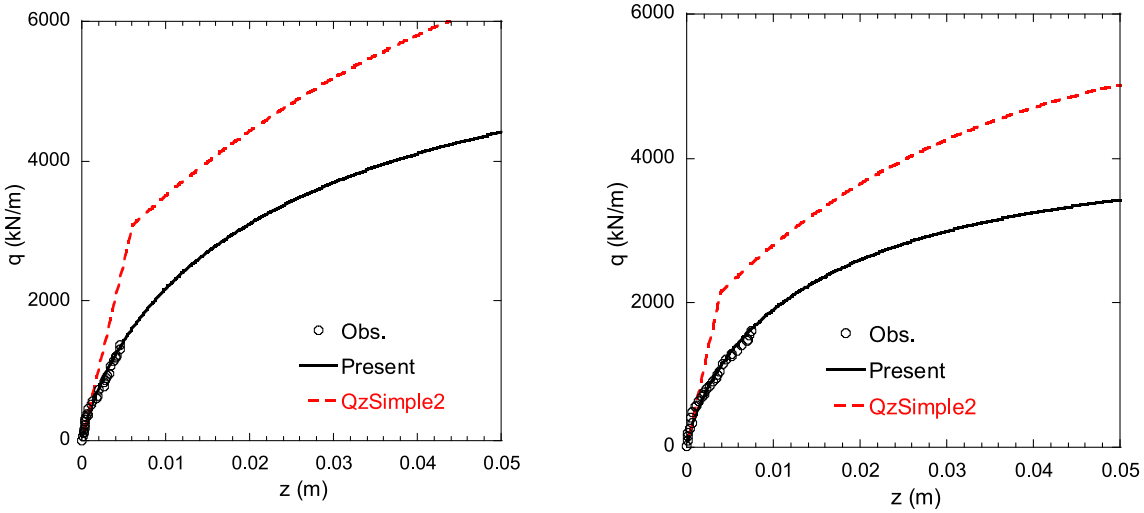

Fig. 3. Predicted and measured q-z backbone curves.

previous QzSimple2 model.

Similarly, Fig. 6 depicts the acceleration responses of bridge deck and the settlement-rotation responses of shallow foundation by the numerical models and experiments under the base excitation of a 12-cycle 2-Hz sine pulse with 0.50 g acceleration amplitude. The ascending slope of the rotation-settlement response proves that the foundation uplift occurs for this excitation level. Therefore, it is adopted to validate the capability of the proposed q-z spring to capture the behavior of foundation uplift. It is found that for the acceleration response of bridge deck, the proposed model and the previous QzSimple2 model predict the responses with almost the same amplitude and very close to the experiment. This slight underestimation after the first period may come from the differences between the targeted and generated waves as mentioned above or the error of measurement caused by scaling factor. The reason why the two numerical models show the same peaks is that the same gap model is used in the two numerical models. Referring to the settlement-rotation response of shallow foundation, the proposed model matches reasonably with the experiment while the previous QzSimple2 model significantly underestimates the settlement response but substantially overestimates the rotation response. This is also caused by the large elastoplastic stiffness and ultimate bearing capacity in QzSimple2 model. Fig. 7 shows the scatter plots for the 0.50 g acceleration amplitude, together with the corresponding validation metric boundary. It is obvious that the proposed model shows better performance for the 0.50 g acceleration amplitude than the previous QzSimple2 model. In summary, both the compression and uplift behaviors of the proposed q-z spring show better performance than those in QzSimple2 model for 0.15 g and 0.50 g acceleration amplitudes, respectively.

4. Seismic loading of wind turbine tower and shallow foundation

The shallow foundation of the No.4 wind turbine at the Aso-nishihara wind farm was cracked during the severe Kumamoto earthquake, which is adopted as the engineering background in this study. Fig. 8 shows the outline of the No. 4 wind turbine, the dimension of shallow

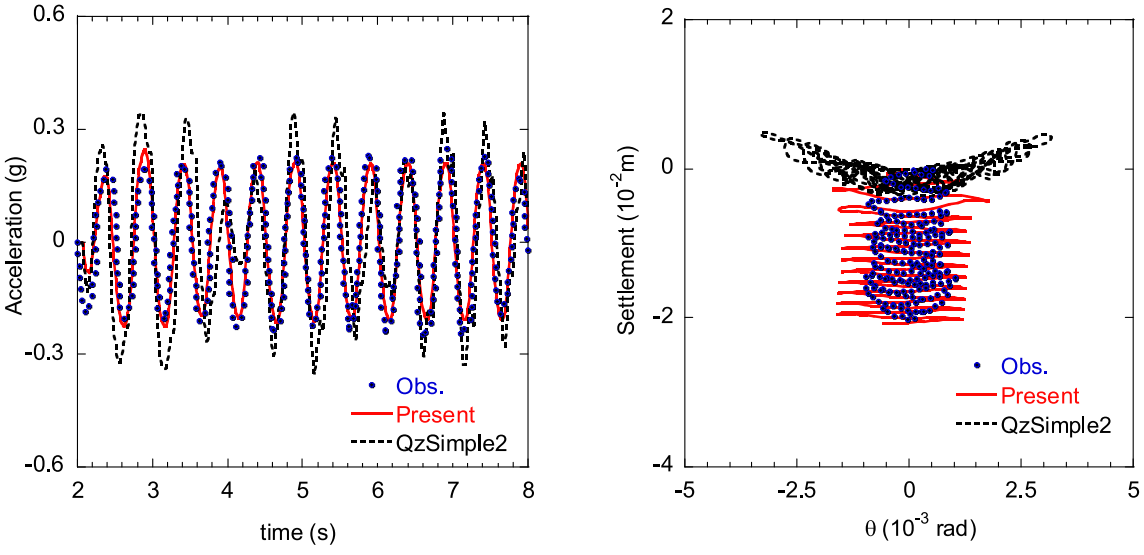

Fig. 4. Comparison of the responses under the base excitation of a 12-cycle 2-Hz sine pulse with a 0.15 g acceleration amplitude.

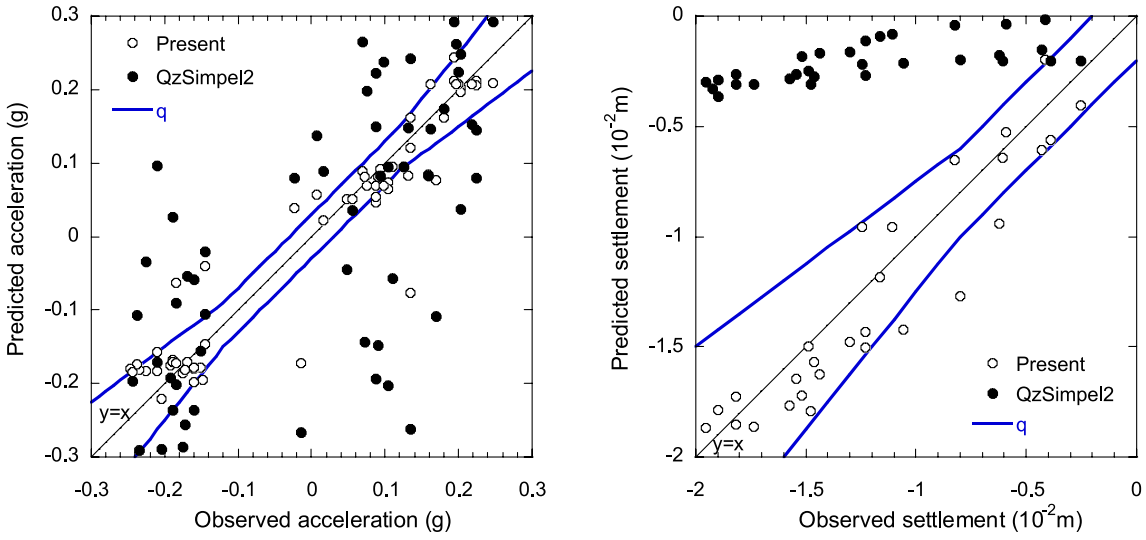

Fig. 5. Scatter plots for comparison between the Winkler model and the experiments for the 0.15 g acceleration amplitude.

foundation and the information of supporting soil. It is a 1.75 MW wind turbine with the hub height of 66.074 m and the rotor diameter of 66 m. The shallow foundation is cruciform-shaped rather than conventionally square-shaped, which has the dimensions of 14.5 m in length, 6 m in width and 1.8 ~ 2.15 m in height. The detail information of the wind turbine is summarized in Table 4. The wind turbine is supported by the layered soil. It contains a clayey rock layer from −1.7 m to −3.0 m (Layer 2), a sandy rock layer from −3.0 m to −6.7 m (Layer 3) and a sandy rock layer from −6.7 m to −13.5 m (Layer 4). Since the height of Layer 1 is 1.7 m while the embeddment of foundation is 2.4 m, the properties of Layer 1 is omitted. The layer under Layer 4 is the engineering bedrock, which is not shown in Fig. 8c. The location of the dangerous section of shallow foundation is marked in both Fig. 8b and 8c, which is crucial to evaluate the safety of shallow foundation. The input seismic wave for the No.4 wind turbine is calculated from the recorded seismic wave at Nishihara Komori by the nonlinear soil dynamic analysis in OpenSees [11]. The acceleration response spectra of recorded and calculated seismic waves are shown in Fig. 9. More information about the wind turbine, the supporting soil and the seismic wave can be found in Reference [3]. Note that the acceleration response spectrum of the seismic wave at the engineering bedrock is also plotted in Fig. 9, which will be used in Section 4.2.

4.1. Effect of foundation uplift on the seismic loading

The effect of foundation uplift on the seismic loading of wind turbine tower and shallow foundation is investigated using two Winkler models. One is the proposed Winkler model (referred as with uplift), in which the foundation uplift is allowed. The other is a linear Winkler model with constant spring stiffness and dashpot damping, in which the foundation uplift is not allowed. The parameters in the equivalent linear Winkler model are derived from the linear sway-rocking model with the assumption of rigid foundation as shown in Appendix B (referred as w/o uplift). Two numerical models are built for the No.4 wind turbine using the proposed Winkler and equivalent linear Winkler models, in which the foundation is modelled as rigid beams since the

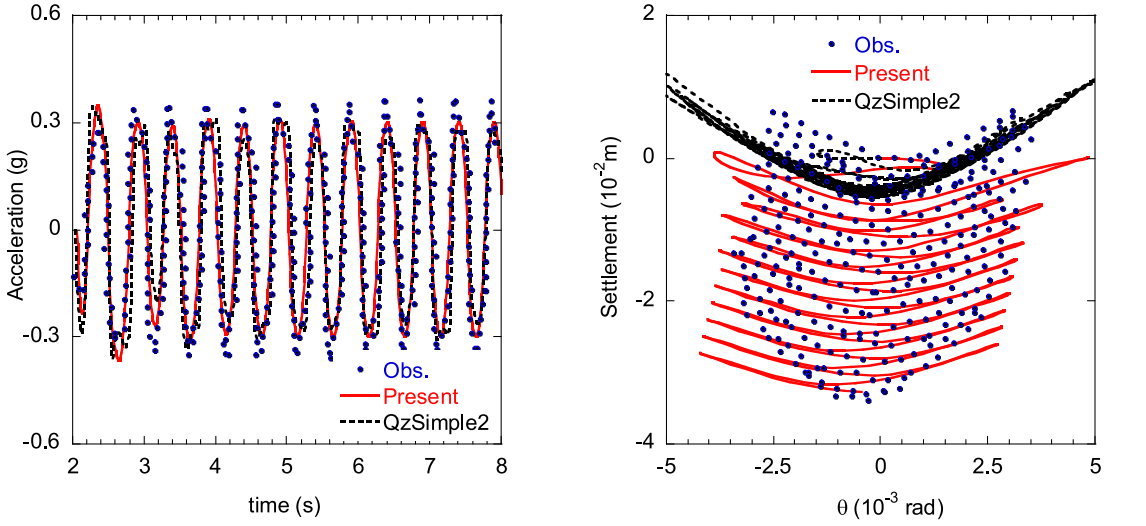

Fig. 6. Comparison of the responses under the base excitation of a 12-cycle 2-Hz sine pulse with a 0.50 g acceleration amplitude.

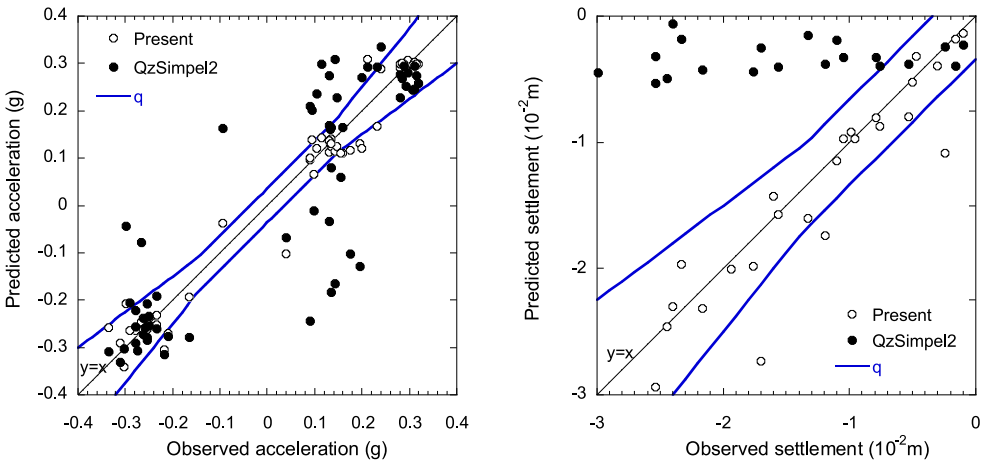

(a) Acceleration response of bridge deck **(b) Settlement-rotation response of foundation**

Fig. 7. Scatter plots for comparison between the Winkler model and the experiments for the 0.50 g acceleration amplitude.

assumption of rigid foundation is adopted when deriving the equivalent linear Winkler model. The rigid beams are approximated by elastic beams with a very large Young's modulus, e.g.$E_{RB} = 10^{10}E_{EB}$ ($E_{EB} = 2.3E + 07$kPa), E_{RB} and E_{EB} are the Young's modulus of rigid and elastic beams respectively. Note that cone model is adopted to convert the layered soil into an equivalent half-sapce (see Ishihara and Wang [39]) since the proposed and equivalent linear Winkler models can only accept one set of parameters. The rotor-nacelle assembly is modeled with a lumped mass and connetted to the tower top by a rigid beam. The tower is modeled with lumped masses and Euler–Bernoulli beam elements. The number of beam elements is 28, which meets the requirement of JSCE guideline [4]. All lumped masses and stiffnesses of beam elements are determined according to the real wind turbine. The structural damping is modeled using the Rayleigh damping model and the structural damping ratio of first mode is 0.2%, which is determined according to the filed measurement of a 2.4 MW wind turbine in Oh and Ishihara [40]. The structural damping ratio of second mode adopts the same value as that of first mode as recommended by JSCE guideline [4]. The two numerical models are also implemented and solved in OpenSees [11] as described in Section 3.3.

The predicted maximum seismic loading on the wind turbine tower with and without considering foundation uplift are presented in Fig. 10 and those on the shallow foundation are plotted in Fig. 11. It is observed that the foundation uplift influences the seismic loading on wind turbine tower and shallow foundation significantly. The maximum moments predicted by the equivalent linear Winkler model is larger than those by the proposed Winkler model for the whole tower, which means the moments of wind turbine tower is overestimated without considering foundation uplift. Considering the shear force of wind turbine tower, the prediction at the tower base by the equivalent linear Winkler model is significantly less than that by the proposed Winkler model, which implies that the shear force of wind turbine tower is significantly underestimated without considering foundation uplift. In terms of the seismic loading on the shallow foundation, the predicted maximum shear forces and moments by the equivalent linear Winkler model are dramatically less than those by the proposed Winkler model for most part of foundations, which demonstrates that the foundation uplift significantly increases the seismic loading on the shallow foundation.

To quantify the effect of foundation uplift, the differences of predicted seismic loading at tower base and the dangerous section of shallow foundation with and without considering foundation uplift are calculated by Eq. (17) and summarized in Table 5. It is found that the predicted moment at tower base with considering foundation uplift is 14% less than that without considering foundation uplift while the predicted moment at the dangerous section of shallow foundation with considering foundation uplift is twice over than that without considering foundation uplift. Therefore, the foundation uplift affects the seismic loading on the shallow foundation much more seriously than on the wind turbine tower, which needs to be considerred in the design of wind turbine supporting structures. It is understandable that when the foundation uplift occurs, the contact area between the shallow foundation and the ground is reduced, which causes the increase of seismic loading on the shallow foundation. Inversely, the foundation uplift releases the constants of tower base somehow, which leads to the decrease of seismic loading on wind turbine tower. Note that the discrepancies of shear force at tower base with and without foundation uplift may be due to the gravity of tower since the wind turbine tower is tilted when the foundation uplift occurs while that at the foundation center may come from the connection between beam elements of wind turbine tower and shallow foundation.

$$Dff_1(x) = \frac{x_{\text{with uplift}} - x_{\text{w/o uplift}}}{x_{\text{wo/ uplift}}} \times 100\% \tag{17}$$

where $Dff_1(x)$ is the difference of x with and without the foundation uplift, $x_{\text{w/o uplift}}$ is the predicted x by the model without considering foundation uplift (equivalent linear Winkler model), $x_{\text{with uplift}}$ is the predicted x by the model considering foundation uplift (proposed Winkler model), x could be shear force or moment at the tower base or at the dangerous section of foundation.

The moment-rotation responses at the tower base are predicted by the equivalent linear Winkler and proposed Winkler models and compared in Fig. 12. Two predictions by the proposed Winkler model are plotted in Fig. 12, one uses a rigid foundation and the other uses an elastic–plastic foundation with crack. It is observed that the moment-rotation response without considering the foundation uplift is almost linear while those with considering the foundation uplift are S-shaped, which implies that the foundation uplift does occur for the targeted wind turbine. When the foundation uplift occurs, the maximum moment is reduced and remains constant, but the maximum rotation increases dramatically. This is also because the constraint of the shallow

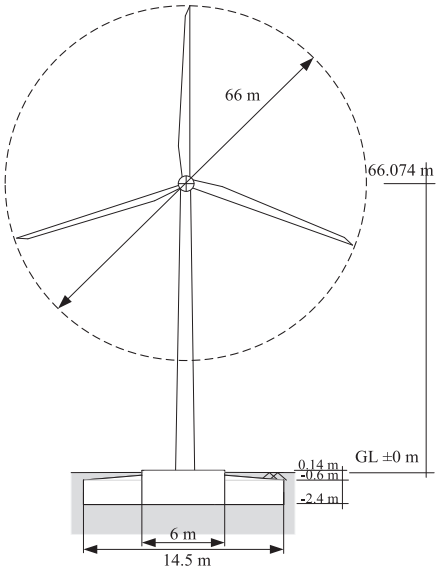

(a) Outline of the whole system

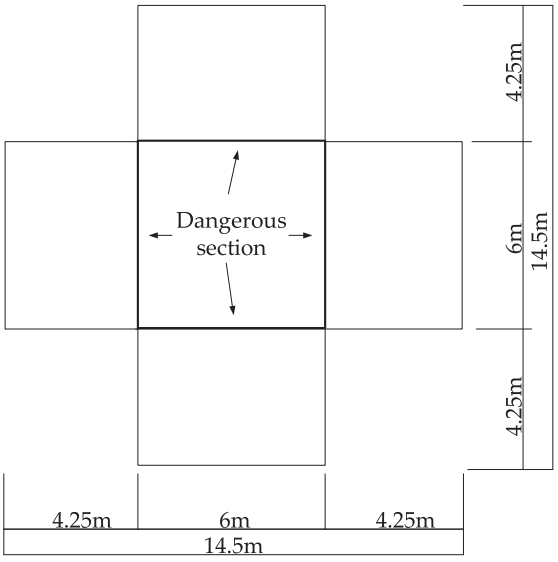

(b) Top view of shallow foundation

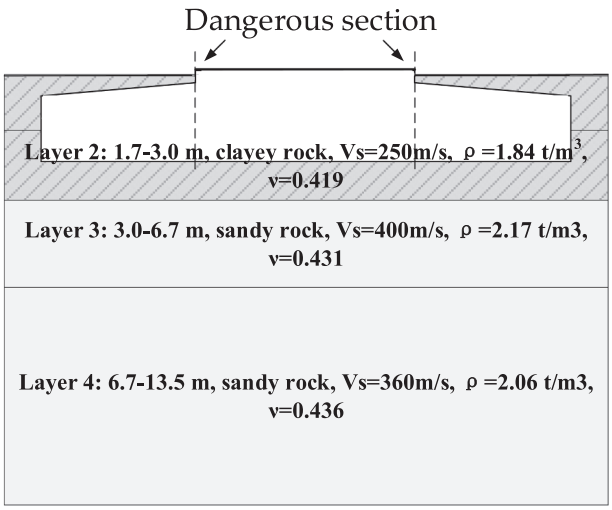

(c) Detail information of shallow foundation

Fig. 8. The No. 4 wind turbine.

Table 4
Summary of the No.4 wind turbine.

Description	Value
Name	Vestas V66
Rating	1.75 MW
Hub height (above G.L)	66.074 *m*
Rotor diameter	66 *m*
Tower diameter, thickness	2.314 ~ 4.028 m, 0.012 ~ 0.028 *m*
Nacelle & rotor mass	84,100 kg
Tower mass (with equipments)	98,800 kg
Foundation shape, dimension	Cruciform shaped, Concrete 6 m × 14.5 m × (1.8 ~ 2.15) m, Steel D25@200 (top & bottom)
Foundation material	Concrete C25, Steel SD-295A

foundation by the ground is released somehow. Considering the real condition of wind turbine, the shallow foundation will be deformed or even cracked, which intensifies the evolution of S-shaped moment-rotation response. It is noted that the hysteretic loops of the moment-rotation response are quite narrow, this is because the supporting soil is quite stiff as shown in Fig. 8c.

4.2. Effect of soil properties on foundation uplift

A sensitivity analysis study is performed to investigate the effect of soil properties on foundation uplift by changing the stiffness of supporting soil. The information of turbine, tower as well as shallow foundation keeps the same as those of the No.4 wind turbine and the configuration of the changeable soil stiffness is illustrated in Fig. 13. 5 representative soil stiffnesses are investigated, which are scaled from a typical soil type Soil I. The information of Soil I [41] is summarized in Table 6. The S-wave velocity and P-wave velocity of each layer (except the bedrock) are scaled with different scaling factors to match the equivalent S-wave velocity for each soil case. The equivalent S-wave

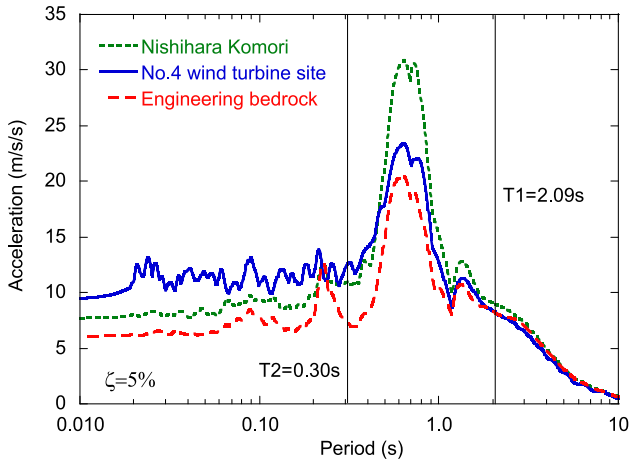

Fig. 9. Comparison of acceleration response spectra of seismic waves at Nishihara Komori, No.4 wind turbine site and engineering bedrock with the damping ratio of 5%

velocity of each soil case is calculated by using Cone model [39]. The equivalent S-wave velocity and scaling factor of each soil case are shown in Table 7. The nonlinear geotechnical properties of Soil I and the scaled soils can be modelled by Hardin-Drnevich model with the reference shear strain $\gamma_{0.5}$ of 0.10% for sand and 0.18% for clay and maximum damping ratio h_{max} of 21% for sand and 17% for clay as shown in JSCE guideline [4]. The seismic wave at engineering bedrock is back-calculated by using the recorded Kumamoto earthquake at Nishihara Komori, whose acceleration response spectrum with the damping ratio of 5% is shown in Fig. 9.

Similar to Section 4.1, two numerical models with the proposed and Winkler models are built and solved for each soil case in OpenSees [11]. The predicted maximum seismic loading at the base of wind turbine tower are plotted in Fig. 14 while those at the dangerous section of shallow foundation are plotted in Fig. 15. The corresponding differences between the predictions by the two models are summarized in Table 8. It is noticed that the strong foundation uplift occurs for all soil cases, and large differences exist in the moment at the dangerous section of shallow foundation with and without considering the foundation uplift (see Fig. 15b). It is confirmed that for all soil stiffnesses, the foundation uplift reduces the moment at the tower base but increases the moment at the foundation dangerous section. However, the effect of foundation uplift on the shear forces strongly relies on the supporting soil stiffness. The foundation uplift reduces the shear forces at both the tower base and foundation dangerous section for the softer soil but increases those for the stiffer soil. Since the moment is dominant for the safety of wind turbine supporting structures, the reason why the 90% foundations were cracked but all the towers were safe at the Asonishihara wind farm is revealed.

4.3. Effect of earthquake intensity on foundation uplift

Since the intensity of Kumamoto earthquake is much larger than that of design requirement[3], the effect of earthquake intensity on foundation uplift is investigated to support the design of wind turbine. The influence of earthquake intensity on the response of uplifting structures is also investigated in previous researches (e.g. Yim and Chopra [42], Xu and Spyrakos [43], Chen and Lai [44], Drosos et al. [34], Qin et al. [45]). In this section, a series of analyses are performed with three artificial seismic waves, in which the numerical models of the whole wind turbine are the same as those in Section 4.1. These artificial seismic waves are generated according to the level II earthquake in the JSCE guideline [4], whose acceleration spectra are shown in Fig. 16 with the damping ratio of 5%. The generated seismic waves also fulfill the requirement of IEC61400-1 [46] which states that the ground acceleration corresponding to a 475-year recurrence period should be considered for the seismic loading evaluation of wind turbine. It is obvious that the intensity of the three generated seismic waves are much less than that of Kumamoto earthquake. The predicted maximum seismic loading at the base of wind turbine tower are depicted in Fig. 17 and those at the dangerous section of shallow foundation are portrayed in Fig. 18. The maximum results of the three seismic waves are picked up to evaluate the effect of foundation uplift under the level II earthquake. The differences of predicted seismic loading with and without considering foundation uplift are calculated by Eq. (17) and summarized in Table 9. It is noticed that significant differences exist for the moment at foundation dangerous section especially for large soil stiffnesses, which means that the foundation uplift does occur for the designed earthquake intensity. Therefore, it is necessary to consider the effects of foundation uplift in the real design.

5. Conclusion

The effects of foundation uplift on the seismic loading of wind turbine tower and shallow foundation are investigated by using a new dynamic Winkler model. Some results obtained from a limited number of solutions and conclusions are summarized:

A new dynamic Winkler model is proposed for the dynamic response

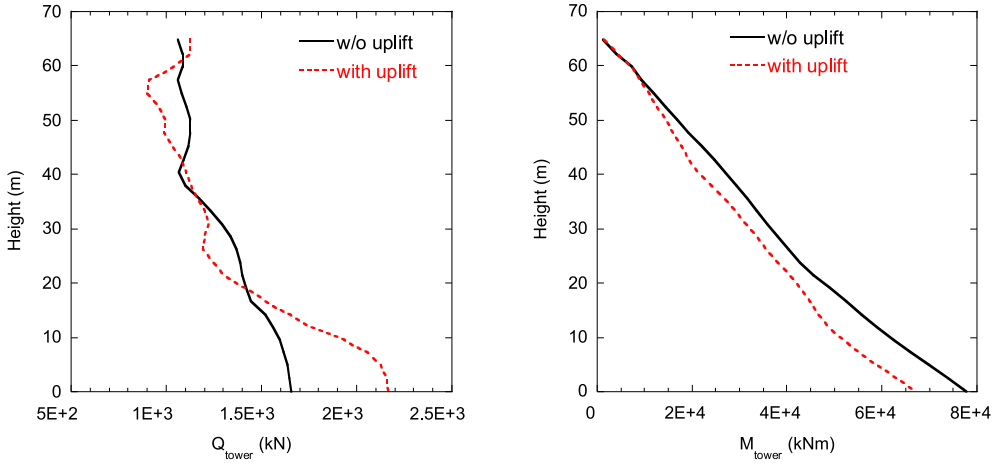

(a) Maximum shear force **(b) Maximum moment**

Fig. 10. Comparison of seismic loading on wind turbine tower with and without foundation uplift.

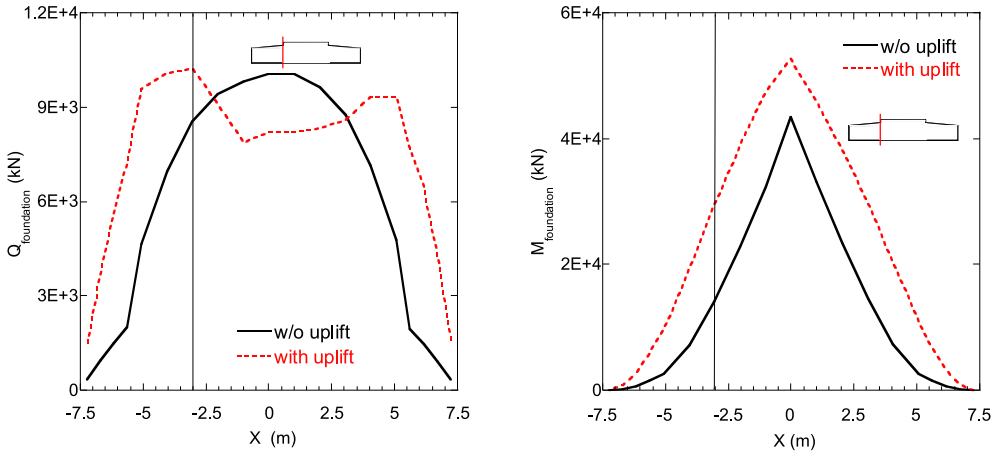

(a) Maximum shear force **(b) Maximum moment**

Fig. 11. Comparison of seismic loading on shallow foundation with and without foundation uplift.

Table 5
Differences of seismic loading predictions between with and without foundation uplift.

	Tower base		Foundation dangerous section	
	shear force	moment	shear force	moment
Difference in percentage	31%	−14%	20%	108%

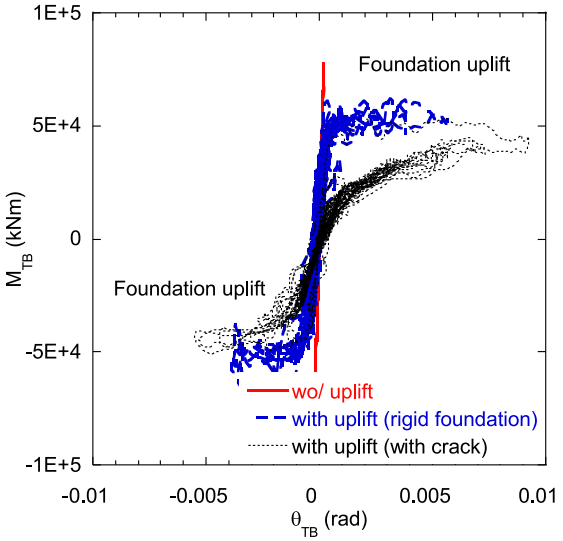

Fig. 12. Comparison of moment-rotation response with and without foundation uplift.

analysis of shallow foundation by applying the PySimple3 model to replace the elastoplastic component in QzSimple2 for the compression under the foundation and the gap model in QzSimple1 to capture the foundation uplift and is named as QzSimple4 in this study.

The predicted backbone curves by the proposed QzSimple4 model shows good agreement with those by experiments, while the conventional QzSimple2 model significantly overestimates the linear range and ultimate bearing capacity. In addition, the proposed model reasonably captures the acceleration responses of the bridge deck and the settlement-rotation responses of shallow foundation under various excitation levels. However, the conventional model obviously

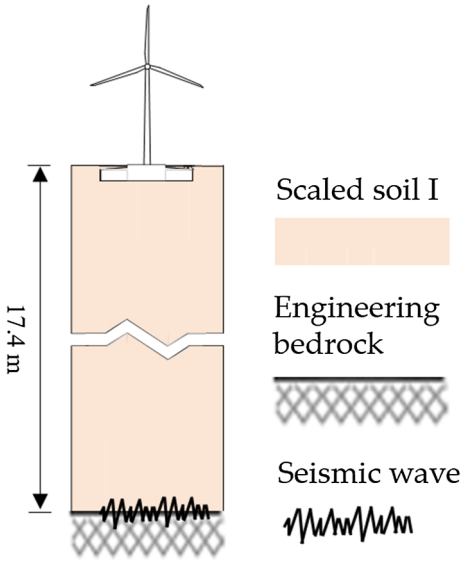

Fig. 13. Shallow foundation supported wind turbines with scaled Soil I.

Table 6
Summary of Soil I [41]

No. of layer	Depth$D$ (m)	Densityρ (t/m^3)	S-wave velocity V_S (m/s)	P-wave velocity V_P (m/s)	Soil type
1	3.0	1.7	130	320	Sand
2	5.7	1.8	340	720	Sand
3	10.0	1.7	280	720	Clay
4	17.4	1.9	380	1980	Sand
Bedrock	–	2.1	510	1980	Rock

Table 7
Equivalent S-wave velocity and scaling factor of 5 soil cases.

Soil case	1	2	3	4	5
Equivalent S-wave velocity $V_{S,\,equivelent}$ (m/s)	200	250	300	356	400
Scaling factor	0.54	0.69	0.83	1	1.15

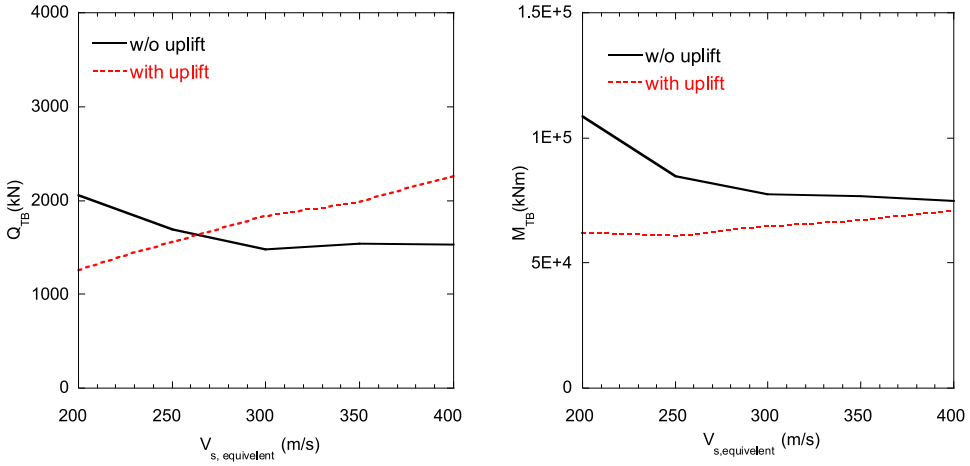

(a) Maximum shear force at tower base **(b) Maximum moment at tower base**

Fig. 14. Effect of foundation uplift on seismic loading of wind turbine tower with various soil stiffnesses.

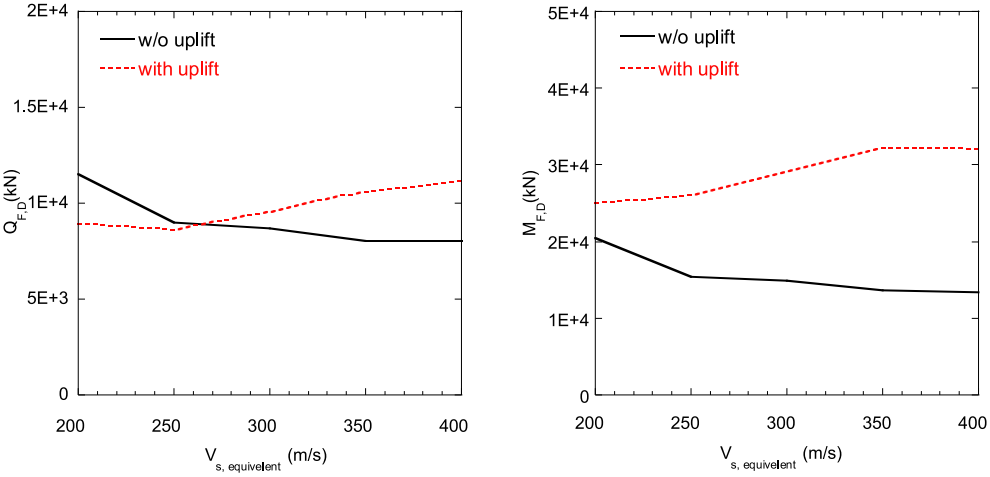

(a) Maximum shear force at foundation dangerous section **(b) Maximum moment at foundation dangerous section**

Fig. 15. Effect of foundation uplift on seismic loading of shallow foundation with various soil stiffnesses.

Table 8
Differences of seismic loading predictions with variable soil properties.

$V_{S,equivalent}$ (m/s)	200	250	300	350	400
Difference of shear force at tower base	−39%	−8%	24%	29%	48%
Difference of moment at tower base	−43%	−28%	−16%	−12%	−5%
Difference of shear force at foundation dangerous section	−23%	−5%	10%	32%	39%
Difference of moment at foundation dangerous section	23%	68%	95%	137%	139%

overestimates some acceleration responses of the bridge deck and significantly underestimates the settlement responses of shallow foundation.

The foundation uplift occurs under severe earthquakes. Without considering the foundation uplift, the moment on the wind turbine tower is slightly overestimated, while that on the shallow foundation is significantly underestimated for large soil stiffnesses.

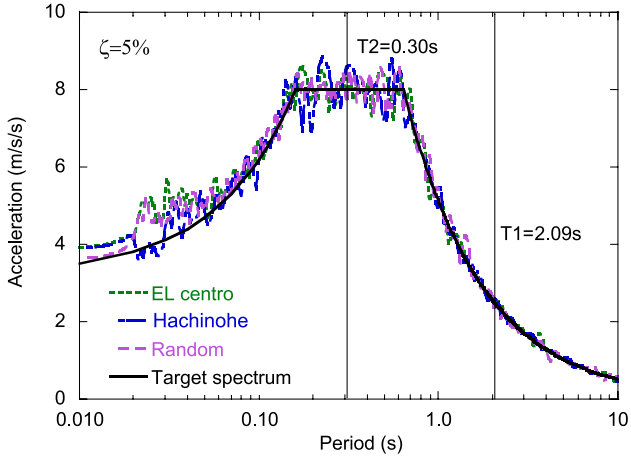

Fig. 16. Acceleration response spectra of generated seismic waves with the damping ratio of 5%

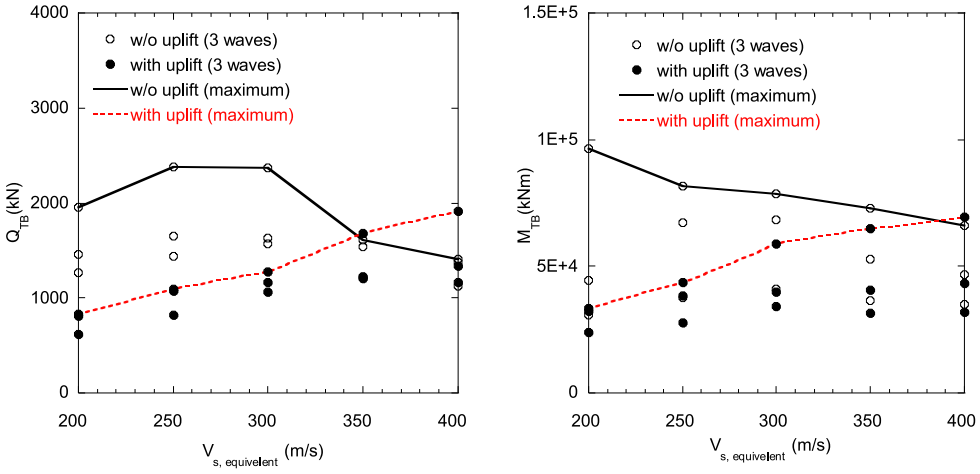

(a) Maximum shear force at tower base **(b) Maximum moment at tower base**

Fig. 17. Comparison of seismic loading of wind turbine tower with Level II earthquakes.

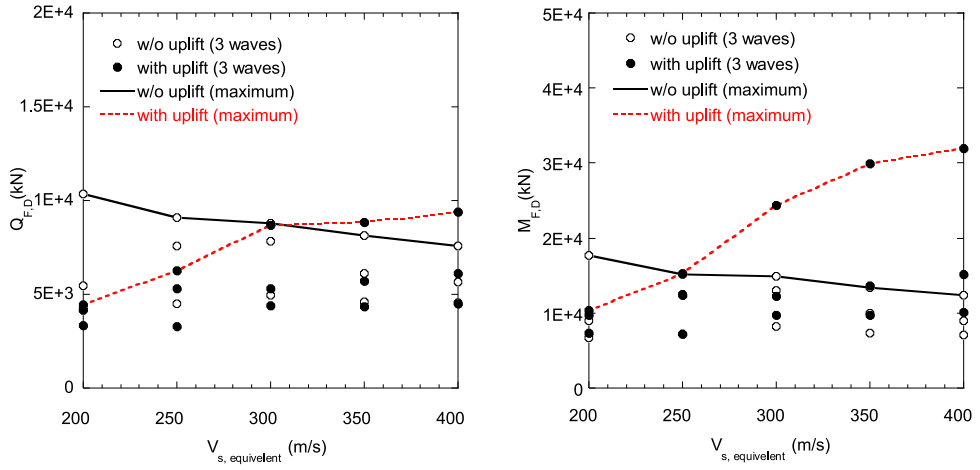

(a) Maximum shear force at foundation dangerous section **(b) Maximum moment at foundation dangerous section**

Fig. 18. Comparison of seismic loading of shallow foundation with Level II earthquakes.

Table 9
Differences of seismic loading predictions with Level II earthquakes.

$V_{S,equi}$(m/s)	200	250	300	350	400
Difference of shear force at tower base	−57%	−54%	−46%	5%	36%
Difference of moment at tower base	−65%	−46%	−25%	−11%	5%
Difference of shear force at foundation dangerous section	−57%	−31%	−1%	9%	24%
Difference of moment at foundation dangerous section	−41%	1%	64%	123%	158%

Acknowledgement

This research was carried out as a part of the joint program funded by J-POWER, Shimizu Corporation, Toshiba Energy Systems & Solutions Corporation, MHI Vestas Offshore Wind Japan and ClassNK. The authors express their deepest gratitude to the concerned parties for their assistance during this study.

Author Contributions

This study was performed as a part of Lilin Wang's doctoral research supervised by Takeshi Ishihara. Lilin Wang and Takeshi Ishihara designed the structure of the paper and wrote the paper.

Conflicts of Interest

The authors declare no conflict of interest.

Appendix A. The way to derive the experimental q-z backbone curves in Fig. 3

The experimental q-z backbone curve in Fig. 3 (known as Obs.) can be derived from the moment-rotation and settlement-rotation responses corresponding to the Aegion seismic wave as shown in Fig. A1. The data between the two marks are adopted to derive the moment-settlement response for both large foundation and medium foundation in Fig. A2. Note that the settlement in Fig. A2 is revised as positive values. Once the moment-settlement response is available, the experimental q-z backbone curve in Fig. 3 (known as Obs.) can be obtained by Eq. (A1). Note that Eq. (A1) is analogy to the formula calculating the maximum moment capacity in Allotey and El Naggar [7] as shwon in Eq.(A2). The analogy works since it is believed that Eq. (A2) suits not only the maximum moment capacity in the ultimate state but also other moments.

$$q = \frac{N^2}{NL - 2M} - \frac{N}{L} \tag{A1}$$

$$M_u = \frac{NL}{2} - \frac{N^2}{2q_u} \tag{A2}$$

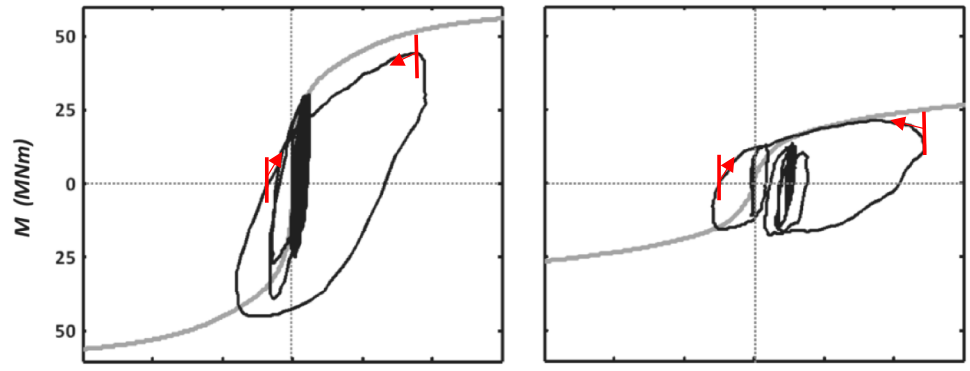

(a) Moment-rotation response: Large foundation (left) and Medium foundation (right)

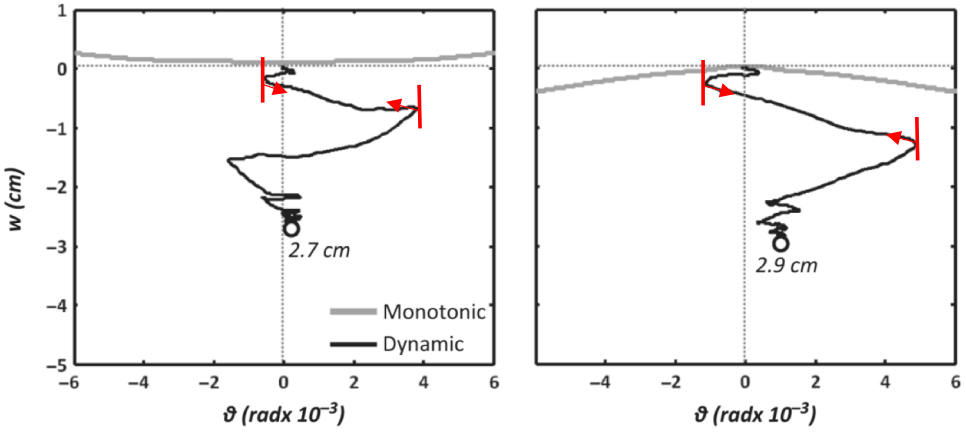

(b) Settlement-rotation response: Large foundation (left) and Medium foundation (right)

Fig. A1. Foundation responses under the Aegion seismic wave [26]

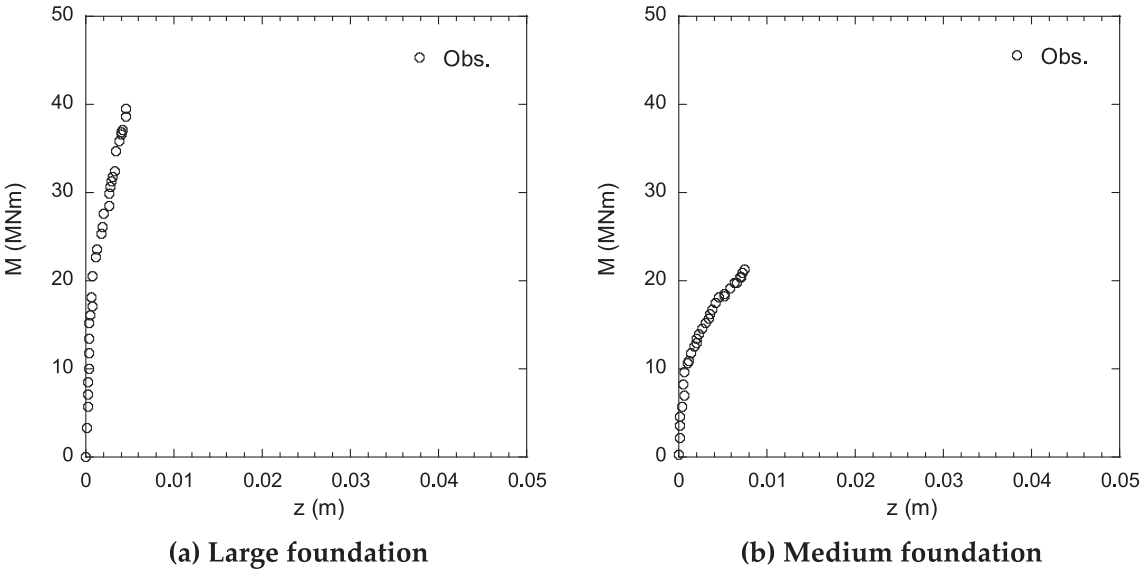

Fig. A2. Derived moment-settlement responses under the Aegion seismic wave.

Appendix B. An equivalent linear Winkler model derived from the SR model

The spring distribution in the equivalent linear Winkler model for a shallow foundation with the length D and the width B is shown in Fig. B1. Assume the shallow foundation is rigid and has a small rotational displacement θ, the restoring moment acting on the shallow foundation by the soil springs ($M_{\text{el - Winkler}}$) can be calculated by Eq. (B1). If the equivalent linear SR model is adopted for the same shallow foundation, the restoring moment ($M_{\text{el - SR}}$) is calculated by Eq. (B2). Then, total vertical spring stiffness in the equivalent linear Winkler model can be derived by equating the two restoring moments as shown in Eq. (B3). The horizontal spring stiffness is the same as that in the equivalent linear SR model. Similarly, the dashpot damping in the Winkler model can be obtained as shown in Eq. (B4).

$$\begin{aligned} M_{\text{el - Winkler}} &= \sum_{i=1}^{N} F_i \cdot x_i = \sum_{i=1}^{N} (k_v \cdot B \cdot dx \cdot \delta_i) \cdot x_i \\ &= \sum_{i=1}^{N} (k_v \cdot B \cdot dx \cdot (\theta \cdot x_i)) \cdot x_i = \theta k_v B \sum_{i=1}^{N} x_i^2 dx = 2\theta k_v B \int_0^{D/2} x^2 dx \\ &= \theta \cdot k_v \cdot \left(\frac{BD^3}{12}\right) = \theta \cdot k_v \cdot I_y = \theta \cdot \frac{K_v}{A} \cdot I_y = \theta K_v \frac{I_y}{A} \end{aligned} \tag{B1}$$

$$M_{\text{el - SR}} = \theta \cdot K_r \tag{B2}$$

$$K_v = K_r \frac{A}{I_y} \tag{B3}$$

$$C_v = C_r \frac{A}{I_y} \tag{B4}$$

Here, $F_i = k_v \cdot B \cdot dx \cdot \delta_i$, $\delta_i = \theta x_i$, $I_y = \frac{BD^3}{12}$, $k_v = \frac{K_v}{A}$ and $A = BD$.

where F_i is the restoring force of the i^{th} spring, δ_i is the displacement of the i^{th} spring, x_i is the distance between the foundation center and the i^{th} spring, k_v is the vertical spring stiffness of unit area of shallow foundation, K_v and C_v are the vertical spring stiffness and dashpot damping of the whole foundation in the equivalent linear Winkler model while K_r and C_r are the rotational spring stiffness and dashpot damping in the equivalent linear SR model, A and I_y are the area and the second moment of area, respectively.

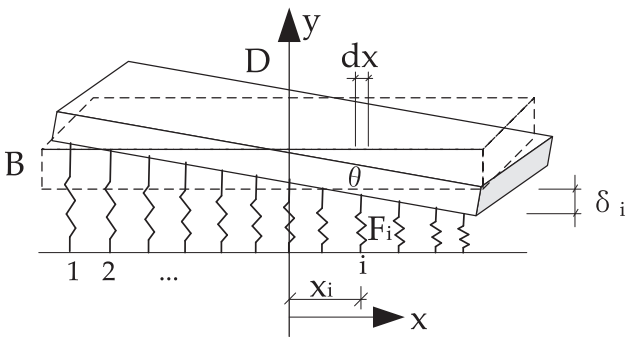

Fig. B1. Vertical spring distribution in the equivalent linear Winkler model.

References

[1] DNVGL-ST-0126: Support structures for wind turbines. Oslo, Norway: DNV, 2016.
[2] Allotey N, Naggar MH. A consistent soil fatigue framework based on the number of equivalent cycles. Geotech. Geol. Eng. 2008;26(1):65.
[3] J-Wind Service Co. L. Accident survey report. 2018. (in Japanese) https://www.meti.go.jp/shingikai/sankoshin/hoan_shohi/denryoku_anzen/newenergy_hatsuden_wg/pdf/013_03_02.pdf.
[4] Ishihara T, editor. Guidelines for design of wind turbine support structures and foundations (In Japanese); 2010.
[5] Chatzigogos CT, Pecker A, Salençon J. Macroelement modeling of shallow foundations. Soil Dyn. Earthquake Eng. 2009;29(5):765–81.
[6] Figini R, Paolucci R, Chatzigogos C. A macro-element model for non-linear soil–-shallow foundation–structure interaction under seismic loads: theoretical development and experimental validation on large scale tests. Earthquake Eng. Struct. Dyn. 2012;41(3):475–93.
[7] Allotey N, El Naggar MH. Analytical moment–rotation curves for rigid foundations based on a Winkler model. Soil Dyn. Earthquake Eng. 2003;23(5):367–81.
[8] Allotey N, El Naggar MH. Generalized dynamic Winkler model for nonlinear soil–structure interaction analysis. Can. Geotech. J. 2008;45(4):560–73.
[9] Allotey N, El Naggar MH. An investigation into the Winkler modeling of the cyclic response of rigid footings. Soil Dyn. Earthquake Eng. 2008;28(1):44–57.
[10] Raychowdhury P, Hutchinson TC. Performance evaluation of a nonlinear Winkler-based shallow foundation model using centrifuge test results. Earthq Eng Struct Dyn. 2009;38(5):679–98.
[11] McKenna F. OpenSees: a framework for earthquake engineering simulation. Comput. Sci. Eng. 2011;13(4):58–66.
[12] Boulanger RW. The PySimple1 Material, Document for the OpenSees platform. 2000. http://opensees.berkeley.edu.
[13] Boulanger RW. The QzSimple1 Material, Document for the OpenSees platform. 2000. http://opensees.berkeley.edu.
[14] Boulanger RW. The TzSimple1 Material, Document for the OpenSees platform. 2000. http://opensees.berkeley.edu.
[15] Boulanger RW, Curras CJ, Kutter BL, Wilson DW, Abghari A. Seismic soil-pile-structure interaction experiments and analyses. J. Geotech. Geoenviron. Eng. 1999;125(9):750–9.
[16] Choi JI, Kim MM, Brandenberg SJ. Cyclic p-y Plasticity Model Applied to Pile Foundations in Sand. J. Geotech. Geoenvironmental Eng. 2015;141(5):04015013.
[17] Katsanos EI, Thöns S, Georgakis C. Wind turbines and seismic hazard: a state-of-the-art review. Wind Energy 2016;19(11):2113–33.
[18] Bazeos N, Hatzigeorgiou GD, Hondros ID, Karamaneas H, Karabalis DL, Beskos DE. Static, seismic and stability analyses of a prototype wind turbine steel tower. Eng. Struct. 2002;24(8):1015–25.
[19] Zhao X, Maißer P. Seismic response analysis of wind turbine towers including soil-structure interaction. Proceedings of the Institution of Mechanical Engineers, Part K: Journal of Multi-body Dynamics 2006;220(1):53–61.
[20] Umar Ahad B, Ishihara T. Seismic load evaluation of wind turbine support structures considering low structural damping and soil structure interaction. Proc. of EWEC. 2012:1–9.
[21] Jardine RJ. Geotechnics, energy and climate change: the 56th Rankine Lecture. Géotechnique 2020;70(1):3–59.
[22] Czerewko MA, Bastekin A, Tunnicliffe J, O'rourke R. Wind turbine construction in and around Carsington Pasture in Derbyshire; overcoming the challenges posed by difficult ground conditions. Q. J. Eng. Geol. Hydrogeol. 2019;52(4):459–80.
[23] Cabalar AF, Uyan RS, Akbulut N. A Study of Foundation Design for Wind Turbines in Hasanbeyli Turkey. Soil Mechanics and Foundation Engineering 2016;53(5):298–303.
[24] Schneider JA, Senders M. Foundation design: A comparison of oil and gas platforms with offshore wind turbines. Mar. Technol. Soc. J. 2010;44(1):32–51.
[25] Vucetic M, Dobry R. Effect of soil plasticity on cyclic response. J Geotech Eng. 1991;117(1):89–107.
[26] Turner B. Kinematic Pile-Soil Interaction in Liquefied and Nonliquefied Ground. Ph. D. Thesis. 2016:422p. https://escholarship.org/uc/item/24v817mp.
[27] Meyerhof GG. Some Recent Research on the Bearing Capacity of Foundations. Can. Geotech. J. 1963;1(1):16–26.
[28] Gazetas G. Foundation Vibrations BT Foundation Engineering Handbook. 1991.
[29] Kagawa T, Kraft LM. Seismic p-y response of flexible piles. J Geotech Eng Div. 1980;106(GT8):899–918.
[30] Darendeli MB. Development of a new family of normalized modulus reduction and material damping. Ph.D. Thesis. 2001::362p.
[31] Raychowdhury P. Nonlinear Winkler-based shallow foundation model for performance assessment of seismically loaded structures. Ph.D. Thesis. 2015:294p. https://escholarship.org/uc/item/6b7322bj.
[32] Vesic AS, Banks DC, Woodard JM. An experimental study of dynamic bearing capacity of footings on sand. In: Sixth Int. Conf. Soil Mech. Found. Eng. Montreal, Canada; 1965:1-18.
[33] Carroll WF. Dynamic Bearing Capacity of Soils: Vertical Displacement of Spread Footing on Clay: Static and Impulsive Loadings. U.S. Army Engineer Waterways Experiment Station, Corps of Engineers, 1963:155p.
[34] Drosos V, Georgarakos T, Loli M, Anastasopoulos I, Zarzouras O, Gazetas G. Soil-Foundation-Structure Interaction with Mobilization of Bearing Capacity: Experimental Study on Sand. J Geotech Geoenvironmental Eng. 2012;138(11):1369–86.
[35] Anastasopoulos I, Loli M, Georgarakos T, Drosos V. Shaking table testing of rocking-isolated bridge pier on sand. J Earthq Eng 2013. https://doi.org/10.1080/13632469.2012.705225.
[36] Anastasopoulos I, Georgarakos T, Georgiannou V, Drosos V, Kourkoulis R. Seismic performance of bar-mat reinforced-soil retaining wall: Shaking table testing versus numerical analysis with modified kinematic hardening constitutive model. Soil Dyn. Earthquake Eng. 2010;30(10):1089–105.
[37] M. Schatzmann, H. Olesen, J. Franke. (Eds.) COST 732 model evaluation case studies: approach and results, COST Office Brussels, 2010.
[38] Oettl D. Quality assurance of the prognostic, microscale wind-field model GRAL 14.8 using wind-tunnel data provided by the German VDI guideline 3783–9. J. Wind Eng. Ind. Aerodyn. 2015;142:104–10.
[39] Ishihara T, Wang L. A study of modal damping for offshore wind turbines considering soil properties and foundation types. Wind Energy 2019;22(12):1760–78.
[40] Oh S, Ishihara T. Structural parameter identification of a 2.4 MW bottom fixed wind turbine by excitation test using active mass damper. Wind Energy 2018;21(11):1232–8.
[41] Architectural Institute of Japan. Seismic Response Analysis and Design of Buildings Considering Dynamic Soil-Structure Interaction. 2006. (in Japanese).
[42] Yim CS, Chopra AK. Earthquake response of structures with partial uplift on Winkler foundation. Earthquake Eng. Struct. Dyn. 1984;12(2):263–81.
[43] Xu C, Spyrakos CC. Seismic analysis of towers including foundation uplift. Eng. Struct. 1996;18(4):271–8.
[44] Chen XC, Lai YM. Seismic response of bridge piers on elasto-plastic Winkler foundation allowed to uplift. J. Sound Vib. 2003;266(5):957–65.
[45] Qin X, Chen Y, Chouw N. Effect of uplift and soil nonlinearity on plastic hinge development and induced vibrations in structures. Adv. Struct. Eng. 2013;16(1):135–47.
[46] IEC 61400-1. Wind turbine generator systems Part1, Safety requirements. International Electrotechnical Commission, 2019.
[47] Vesic AS. Analysis of ultimate loads of shallow foundations. J Soil Mech Found Div 1973;99(sm1) [In this issue].